*J. Basic. Appl. Chem.*, 8(1)1-12, 2018



ISSN 2090-424X
**Journal of Basic and Applied Chemistry**
*www.textroad.com*

# Electrochemical-Anodization Synthesis of Spinel Cobalt Ferrite Films on Various Substrates from Aqueous Medium

**E. M. Elsayed[1], M. M. Moharam[1], I.A. Ibrahim[1], H.F.Y. Khalil[2] M.R, Hussein[2] and M.M.B. El-Sabbah[2]**

[1]Central Metallurgical Research and Development Institute (CMRDI), P.O. BOX.87 Helwan, Egypt 11421,
[2]Chemistry Department Faculty of Science, Al–Azhar University, Nasr City, Egypt

## ABSTRACT

Nanocrystalline cobalt ferrite ($CoFe_2O_4$) thin films have been prepared using electrodeposition-anodization process. The aim of this research was to study the electrodeposited of CoFe2 alloy from aqueous sulphate bath on different substrates like [platinum(Pt),stainless steel(SS), and copper(Cu)]. $CoFe_2$ alloy was electrodeposited from aqueous sulphate on different substrates, e.g. platinum (Pt), stainless steel (SS), and copper (Cu). The prepared alloy was electrochemically anodized in 1 M KOH solution at room temperature to the analogous hydroxide. Therefore, bath temperature, agitation and current density parameters were investigated for the fabricated $CoFe_2$ alloy. Moreover, the maximum current efficiency of 98 % was obtained on Pt substrate at cathodic current density of 100 mA/cm$^2$ for electrodeposited $CoFe_2O_4$ films. The crystal structure, crystallite size, microstructure and magnetic properties for ferrite films were characterized using scanning electron microscopy (SEM), X-ray diffraction (XRD) and vibrating sample magnetometer (VSM). Increasing the annealing temperature up to 800$^0$C is directly proportional to saturation magnetization of $CoFe_2O_4$ films for Pt (64.33 emu/g), SS (54.7 emu/g), and Cu (54.5 emu/g) substrates.

**KEYWORDS:** Electrodeposition, $CoFe_2O_4$, Current efficiency, Current density, Saturation magnetization.

## 1. INTRODUCTION

Pure and substituted ferrites are widely used in modern technologies including catalysis, environment and renewable energy resources owing to their excellent magnetic, semiconducting and sorption properties [1]. Polycrystalline ferrites doped with divalent metal ions ($M^{2+}$ = Mg, Mn, Zn, Ni, Co, Cu, Cd and/or Fe) have the general formula $MFe_2O_4$. Cobalt doped ferrites could be synthesized by reacting the selected transition metal oxides (MO) with $Fe_2O_3$ in which the cation distribution is described by $(Fe_{1-x}Co_x)_A(Fe_{1-x}Co_{1-x})_BO_4$, a general formula where A and B denote tetrahedral and octahedral sites, respectively [2,3] compared to an almost inverse cation distribution (x ~ 0) in case of $CoFe_2O_4$; in which $Co^{2+}$ ions reside B sites and $Fe^{3+}$ ions is equally distributed among A and B sites [4. 5].

Pulsed laser deposition, [6-9], dip coating [10], sputtering [11], laser ablation [12], vacuum arc evaporation [13], spin coating [14-15] and the sol-gel methods [16] were used to fabricate metal oxides spinel. To obtain crystallization, these techniques involve heating the substrate for several hundred degrees Celsius in which the substrate possess heat resistance and thermal expansion coefficient to high extent to avoid degradation of the deposited materials. On the other hand, irregular film dimensions are mostly produced in addition by products, e.g., to toxic gases [17]. To eliminate the aforementioned problems, electrochemical deposition gain more attention owing to the low cost electrochemical growth of nanocrystalline oxide films and its wide-ranging applications [18,19]. Moreover, it is simple, smooth, non-vacuum technique suitable for preparing electrodes [20-22], it controls the film composition and morphology.

The structure of $CoFe_2O_4$ ferrimagnetic nanoparticles cubic spinel represents a class of soft and large magneto crystalline anisotropic materials and reasonable magnetization. They can serve for high-density magnetic recording media, magnetic resonance imaging (MRI), ferro fluids, [23-25], gas sensing, Li ion batteries, bio-processing and catalytic applications [26-29]. Additionally, cobalt ferrites have been used for lead (II) ion extraction [30] and detection of toxic arsenic in aqueous solution [32], anticorrosive nanoparticles [31]. The properties of $CoFe_2O_4$ depends on particle size, shape, degree of crystallinity and phase purity [4].

***Corresponding Author**: M.M.B. El-Sabbah, Chemistry Department Faculty of Science, Al–Azhar University, Nasr City, Egypt.

The goal of this work is to prepare $CoFe_2O_4$ thin films using aqueous electrochemical deposition method. The electrochemical properties were tested using galvanostatic and cyclic voltammetry techniques. The crystalline- micro- structure, particle size, and magnetic properties of the produced ferrites films were also probed by scanning electron microscope (SEM), X-ray diffraction (XRD), and vibrating sample magnetometer (VSM) techniques.

## 2. Experimental

### 2.1. Film Synthesis

Analytical grade ammonium ferrous sulphate hexa hydrate (Fe $(NH_4)_2$ $(SO_4)_2$.6 $H_2O$), cobalt sulphate hepta hydrate ($CoSO_4 \cdot 7$ $H_2O$) and potassium hydroxide (KOH) were used as starting materials. Electrodepositing experiments were accomplished using freshly prepared solutions. The electrolyte was kept unstirred. The pH value of the solution was justified at 3.5 using 0.5 M $H_3BO_3$. Some organic additives, including0.2M saccharin, was used as a brightening agent. Even the presence of saccharin was helpful to achieving the preferred orientations of the $CoFe_2$ alloy deposition [33]

### 2.2. The electrolytic cell

A standard three-electrode cell was used for electrodeposition and anodization of $CoFe_2O_4$ films. (Pt, SS, and Cu substrates) with (1 $cm^2$) area were used as working electrodes. Platinum ($1cm^2$area) and silver/silver chloride saturated in KCl (Ag/AgCl/sat KCl) $E_0$ = 0.200 mV vs. standard hydrogen electrode (SHE) were used as auxiliary and reference electrodes, respectively. The distance between working and auxiliary electrodes was kept constant (1cm) whereas a galvanostatic mode was used to deposit $CoFe_2$ alloy. The samples preparation conditions are listed in Table 1.

**Table1 Galvanostatic parameters for the synthesis of $CoFe_2$ alloy from sulphate bath.**

| Item | Conditions |
|---|---|
| **Bath composition** | 10mL0.05M$CoSO_4$+10mL0.1 M Fe $(NH_4)_2$ $(SO_4)_2$ |
| **Cathodic Current density (mA/$cm^2$)** | 100 |
| **Deposition time (Sec)** | 300 |
| **Bath temperature (°C)** | 25 |
| **Substrate** | Pt, SS and Cu |

The next step is anodization of deposited film (cobalt iron alloy) in 1 MKOH where the film and Pt- electrode act as an anode and cathode, respectively. Then, the resultant film was washed thoroughly with distilled water and dehydrated in a desiccator under vacuum for at least 2 hrs.

The anodization current density and time were adjusted to get well-adhered oxide films to the substrates electrodeposition synthesis parameters was carried out at room temperature (25°C ) according to the conditions summarized in Table2.

**Table 2: Galvanostatic Conditions of the anodization process for the synthesis of cobalt ferrite thin film.**

| Item | Conditions |
|---|---|
| Electrolyte | 1.0 M KOH |
| Anodic Current density (mA/$cm^2$) | 10 |
| Intercalation time (Sec) | 30 |
| Electrolyte temperature | 25°C |

After anodization, the films were washed with distilled water and annealed after drying. The annealing process was implemented in air at 400 °C, 600 °C, 700 °C and 800 °C for 2 hrs.

### 2.3. Volta metric studies:

Cyclic voltammograms, chronopotentiometeric and galvanostatic studies were performed with a PC-controlled potentiostat (Volta- lab 21). PGP201 potentiostate, Galvanosatate 20 V, 1 A with general generator using the previously mentioned three electrode cell.

### 2.4. Film Characterization

Aided by polarization curves, the deposition potentials were estimated. Cyclic voltammograms were performed with a PC-controlled PGP 201 potentiostate (Volta-lab 21), Galvanosatate 20V, 1A with general generator. Electrodeposition was identified Galvanostatically employing constant currents, from -50 to -130 mA $cm^{-2}$ enhanced to get $CoFe_2$ alloy films with maximum thickness. In which the applied current is divided by macroscopic surface area of the deposit to determine the apparent current densities.

The crystalline phases of the annealed ferrite samples were examined using XRD patterns recorded on a Brucker diffractometer (axis D8) using the Co-K$\alpha$ ($\lambda$ = 1.5406 Å) radiation in the range, 2θ from 20° to 80°. The ferrite particle morphologies were examined by SEM recorded on JEOL, model JSM-5410 and magnetic properties were studied by VSM (Lake shore 7410).

## 3. RESULTS AND DISCUSSION

### 3.1. Cyclic Voltammetry.

Fig. 1(A,B) displayed cyclic voltammograms (CVs) of 0.05M of $CoSO_4$, and Co-$Fe_2$ alloy, respectively, from aqueous sulfate bath on different substrates. Voltammetric studies were carried out from 0 to −4 V using a scan rate of 10 $mVs^{-1}$. The CV of 0.05 M of $CoSO_4$ which deposited on (Pt, SS and Cu) is characterized by one cathodic peak (C) at negative potentials (-1.84 V, -1.77 V and -1.643 V) respectively. This cathodic peak is linked with the deposition of $Co^{+2}$ ions to cobalt metal. Conversely, scanning in the positive direction at potential - 4 V, an anodic peak was obviously showed around -0.91V for deposited film on Pt substrate, -0.767 V for stainless steel and copper substrate. The anodic peak related to the dissolution of Co metal into its ions as ascribed in equation (1) [34]

$$Co^{+2} + 2e^{-} \leftrightarrow Co \qquad (1)$$

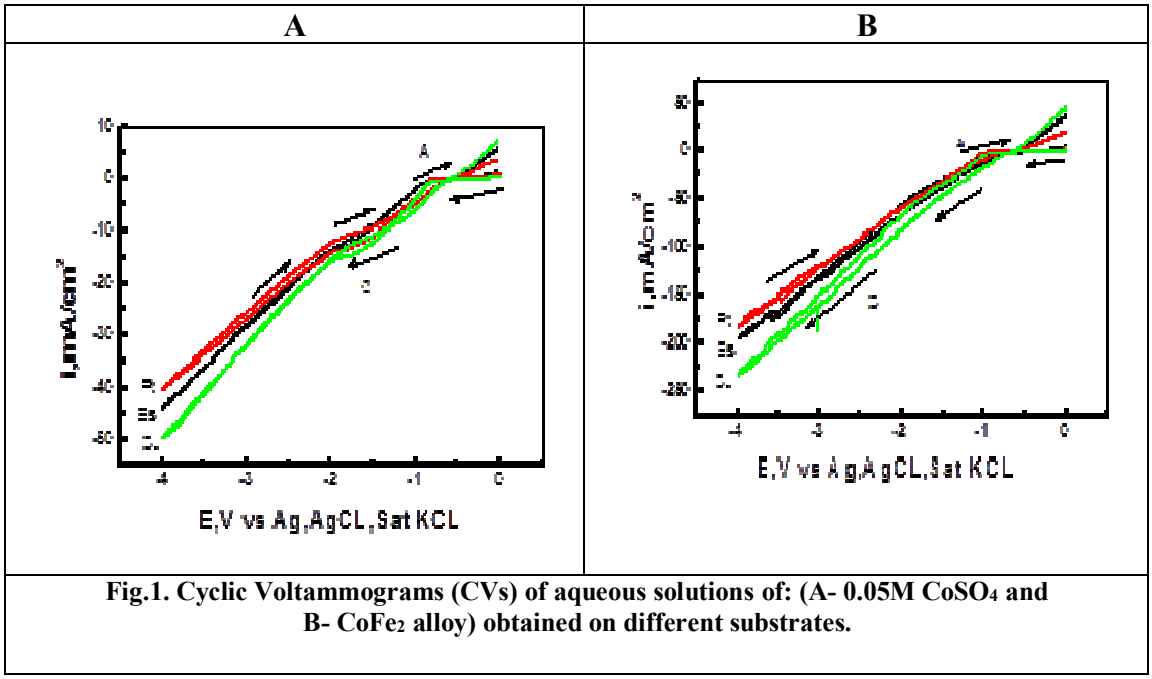


**Fig.1. Cyclic Voltammograms (CVs) of aqueous solutions of: (A- 0.05M $CoSO_4$ and B- $CoFe_2$ alloy) obtained on different substrates.**

### 3.2. LSV for electrodeposition of $CoFe_2$ alloy

#### 3.2.1. Effect of agitation

Fig.2A demonstrates the LSV for electrodeposition of $CoFe_2$ alloy on Pt substrate. Agitating the solution shifted the solution cathodic current density from -220 to -120 $mAcm^{-2}$. The solution agitation rate is inversely proportional to the thickness of the adjacent cathodic layer, which in turn shortens the diffusion path of the deposited metals [35, 36]. Fig.2B reveals the LSV for electrodeposition of $CoFe_2$ alloy on SS substrate. Agitating the solution switched the solution cathodic current density from -175 to -220 $mAcm^{-2}$ [37]. Fig.2C exhibits the LSV for electrodeposition of $CoFe_2$ alloy on Cu substrate. Agitating the solution changed the solution cathodic current density from -160 to -280$mAcm^{-2}$ [38]. Generally, the results show that the deposition current increases with increasing solution agitation but this has opposite effect on the adherence of the deposited film.

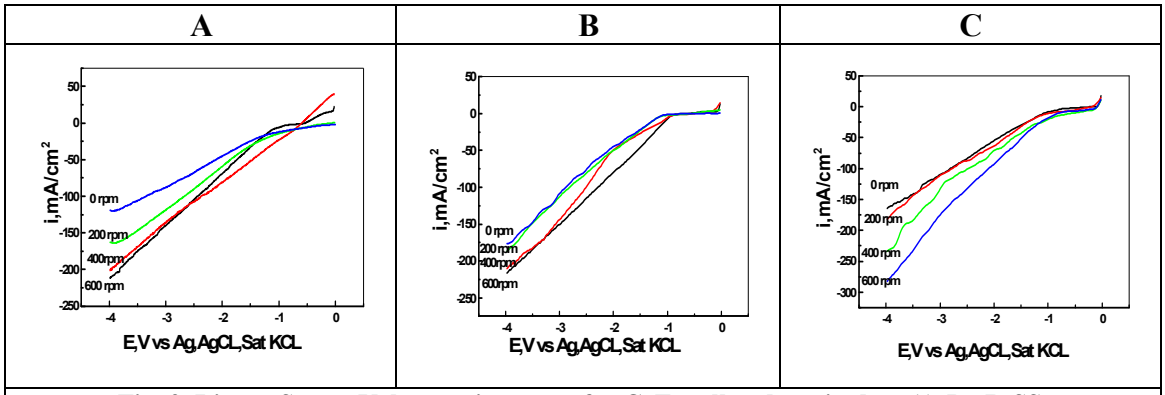


**Fig. 2. Linear Sweep Voltametric curves for $CoFe_2$ alloy deposited on (A-Pt, B-SS, and C- Cu) substrates, SR (10 mV/s), 1 cycle, at different agitation.**

### 3.2.2. Effect of bath temperature.

Fig.3 illuminates the LSV for electrodeposition of $CoFe_2$ alloy on (Pt, S.S. and Cu) substrates. Raising bath temperature from 35 to 50 °C was consequently materialized a reduction in $CoFe_2$ deposition potential from E = -2.108 V, (peak $C_1$) to E = -1.926 V, (peak $C_2$). Certainly, rising bath temperature from 50 to 70 °C was lead to a lack in $CoFe_2$ deposition potential from E =-1.926 V to -1.843. While increasing the bath temperature from 35 to 50 °C during using StSt as working electrode, the deposition potential for $CoFe_2$ alloy was decreased from -2.41 to -2.322 V.

Moreover, raising bath temperature from 50 to 70 °C was lead to a lack in $CoFe_2$ alloy deposition potential from E=-2.322 to -2.23 V. Also, in all cases increasing the solution temperature from 35 to 70 °C increases deposition current density. Alternatively, the deposited films were more adherent, homogeneous, and coherent at room temperature.

Commonly, the elevation in bath temperature increases the grain size which has deposited material and decreases deposition potential. Furthermore, the expansion of bath temperature improves the rate of dissemination and ionic mobility's which develops the conductivity of deposition bath. The lowering in deposition potential with increasing temperature may be because of the expansion in the substance of more respectable metal in the deposited alloy [39].

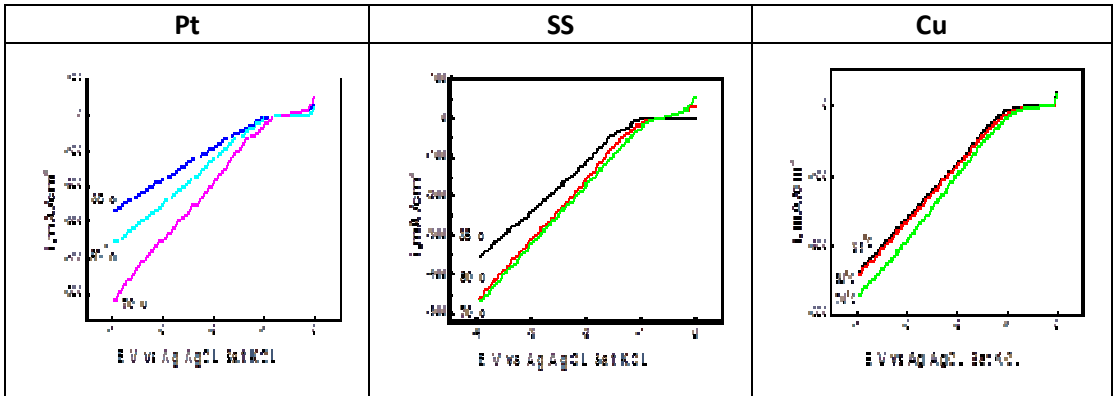


**Fig. 3 Linear Sweep Voltametric curves for $CoFe_2$ alloy deposited on (Pt, SS and Cu) substrates, SR (10 mV/s), 1 cycle, at different bath temperatures .**

### 3.3 Chronopotentiometric study.

Fig.4 demonstrates the glvanostatic curves for electrodepositon of $CoFe_2$ alloy film from aqueous solution of 0.05 M $CoSO_4$ + 0.1 M Fe $(NH_4)_2(SO_4)_2$ on (Pt, SS and Cu) substrates. So to discover the reasonable current density for $CoFe_2$ alloy deposition, the depositions at various current density values -50, -70, -90,-100, -120,-130 and -150 mA $cm^{-2}$ were performed respectively. The potential first growth to a certain extent and then it reduces very fast up to a steady state value. The fast reduction in cathodic potentials shows that the coverage of electrodes surface develops fast. While the steady state indicates that the coverage of electrodes surface is nearly finished [40]. The maximum film thicknesses were (7,1 µm, 6.53 µm and 6.16 µm) for films deposited on (Pt, SS and Cu) substrates respectively at current density -100 $mAcm^{-2}$. Thus, current density of -100 $mA/cm^2$ is found suitable for the deposition of

$CoFe_2$ alloy thin films. Therefore, keeping the current density constant at -100 mA/cm$^2$, the variation in the values of potential with time was noted.

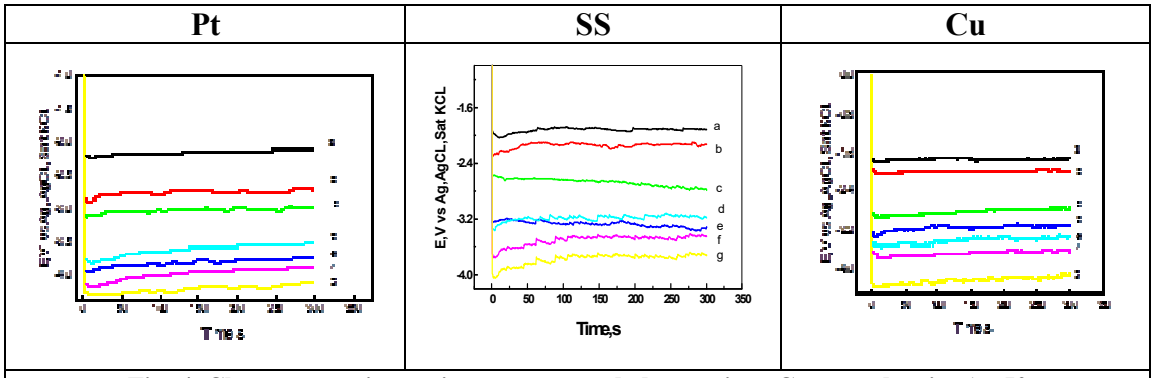


**Fig. 4. Chronopotentiometric curves recorded at various Current density (a−50 mAcm$^{-2}$, b −70 mAcm$^{-2}$, c −90 mAcm$^{-2}$, d−100 mAcm$^{-2}$, e -120 mAcm$^{-2}$, f -130 mAcm$^{-2}$and g −150 mAcm$^{-2}$) for $CoFe_2$ alloy deposited on different substrates.**

### 3.4. Chronoamperometric study.

Fig.5 deduces the variation of current density with time at constant potentials -1.5V, -1,7, -1.9, -2, -2.25, 2.5, 2,750 and -3 V. The value of deposition rate at -2.5V was noticed maximum deposition with high film thickness on Pt substrate. It increases to a certain level and then vastly decreases until reaching a steady state. The fast decrease in potentials shows that the coverage of electrode surface develops fast [41]. Thus, potential (-2.5V) was found suitable for the deposition of thin films on (Pt, SS and Cu) substrates. During the deposition, the steady state of current designates that the coverage of electrode surface is nearly finished.

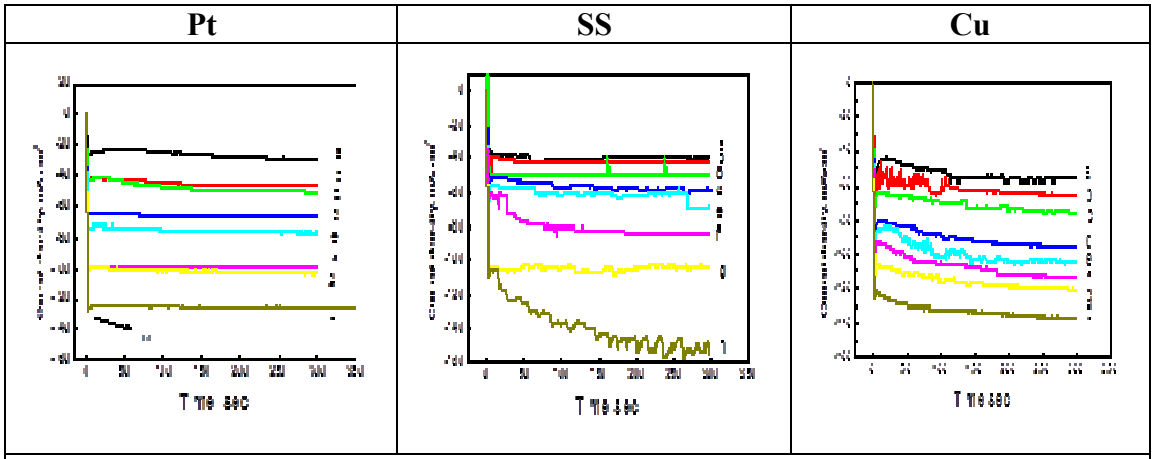


**Fig.5. Chronoamperometric curves for $CoFe_2$ alloy deposited on different substrates. at various deposition potentials (a −1.5 V, b −1.7 V, c −1.9 V, d −2 V, e −2,25 V, f −2.5 V , g −2.750 V and h −3V).**

A model was proposed earlier to describe the initial nucleation process using chronoamperometric technique which could be either progressive or instantaneous depending whether slow growth or fast growth of nuclei, respectively [40,41].

The transients have been assessed by fitting the chronoamperometric curves against the dimensionless theoretical analogues for the diffusion-controlled nucleation (growth of crystals in three dimensions) suggested by Saba et al [42,43]. The demonstrations for the progressive and instantaneous nucleation are given by following equations [43], where $i_{max}$ and $t_{max}$ represents the maximum current density noted at the maximum time $t_{max}$.

$$\frac{I^2_{inst}}{I^2_{max}} = 1.9542 \frac{t_{max}}{t}\left(1 - e^{\frac{-1.2564\ t}{t_{max}}}\right)^2 \quad (2)$$

$$\frac{I^2_{progress}}{I^2_{max}} = 1.2254 \quad \frac{t_{max}}{t}\left(1 - e^{\frac{-2.2367\ t}{t_{max}}}\right)^2 \qquad (3)$$

The similarity of the experimental curves and the theoretical ones could be observed in (Fig.6.). The nucleation and growth of $CoFe_2$ alloy electrodeposited from aqueous media on Pt substrate obey instantaneous mechanism at lower and higher potentials from -1.5 to -3 V.

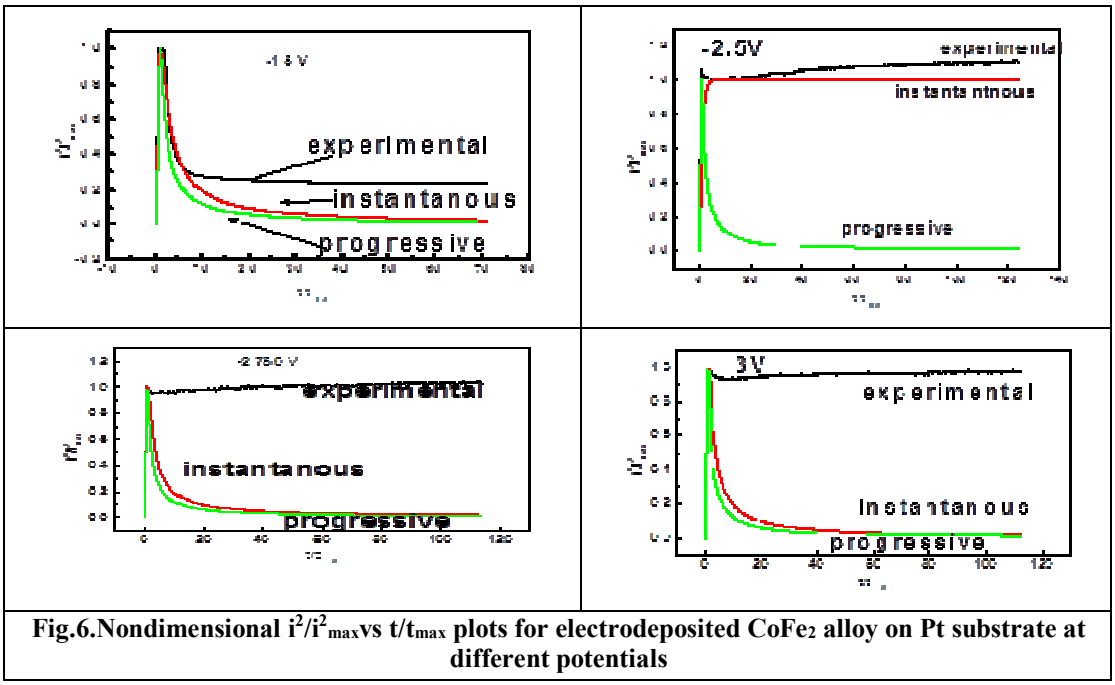


**Fig.6.Nondimensional $i^2/i^2_{max}$ vs $t/t_{max}$ plots for electrodeposited $CoFe_2$ alloy on Pt substrate at different potentials**

### 3.5. Effect of Current density and deposition potential on film thickness.

The thickness of the deposited thin film is unique and directly correlated to preparative parameters; molarity, deposition temperature, deposition time period, rate of deposition, annealing temperature etc. which were substantially improved to get the uniform thin film [44].

$MFe_2$ alloy film thickness was determined using gravimetric precise weight difference in which area and weight of the film was measured, before and after alloy deposition [43-45], the difference of two masses gives the mass of the alloy film and the thickness was obtained by assuming the density of bulk $MFe_2$ as expressed below [46]:

T=mass difference/ρA (4)

Where T is film thickness, ρ is density of M and Fe elements in alloy, and A is total area of electrode surface.

Fig 7 offers plot of $CoFe_2$ alloy film thickness against current density. The results show that, the thickness of the film was 6.7 mm for Pt substrate., 6 mm for st.st and 5,7 mm for Cu at -100 mA $cm^{-2}$. With further increase in deposition current than -100 mA $cm^{-2}$, film thickness was decreased. This is referred to the construction of spongy, vague and less adherent thin film which could have a tensile stress that tends to generate stratum, when it becomes thick [45].

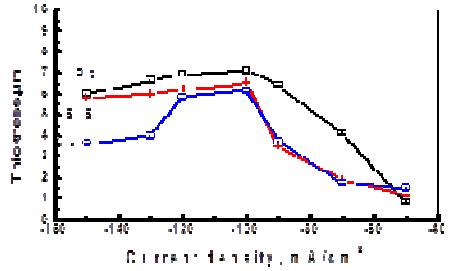

**Fig.7.Variation of film thickness with Current density $CoFe_2$ alloy deposited on different substrates.**

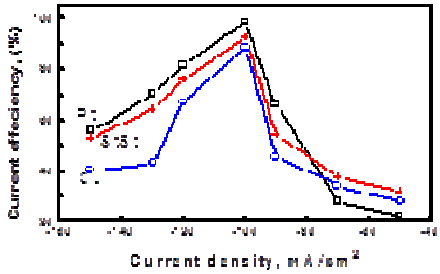

**Fig. 8. Variation of Current efficiency with Current density for $CoFe_2$ alloy deposited on different substrates.**

**3.6. Current efficiency.**

Current efficiency was calculated by dividing the mass of the film deposited on the electrode by the mass expected to be deposited in accordance with Faraday's law [45-48]

$$W = \frac{I \times t_{hr} \times \text{equivalent weight g.}}{26.8 \text{ A. hr.}} \text{ grams} \quad (5)$$

Where:

I: Current intensity in Amperes

If is the $\bar{w}$ weight of metal actually deposited at the cathode, then, current efficiency= $\bar{w}/w * 100(\%)$

Fig.8 reveals the variation of current density with current efficiency on various substrates like Pt, SS, and Cu for 300 second deposition time at room temperature. The maximum current efficiency for $CoFe_2$ alloy is reached to 98.4% with Pt electrode at current density -100 $mAcm^{-2}$. Furthermore, current efficiencies for $CoFe_2$ alloy on both StSt and copper electrodes are 93.9 % and 98.4 % respectively at the same current density -100 $mAcm^{-2}$. At current density lower than -100 $mAcm^{-2}$, the rate of protons reduction is less than that of the metal deposition, if the current density is higher than -100 $mAcm^{-2}$, the rate of the reduction of water molecule increases and hydrogen gas evolved (equations 10-12) [45].

It is supposed that both single metals are reduced in two following steps [48]

$$Co\ (II) + e^- \rightarrow Co(I)_{ads.} \quad (6)$$
$$Co\ (I)_{ads} + e^- \rightarrow Co(S) \quad (7)$$
$$Fe\ (II)\ ) + e^- \rightarrow Fe(I)_{ads.} \quad (8)$$
$$Fe\ (I)_{ads} + e^- \rightarrow Fe(S) \quad (9)$$
$$H^+ + e^- \rightarrow 1/2H_2 \quad (10)$$
$$H_2O + e^- \rightarrow 1/2\ H_2 + OH^- \quad (11)$$
$$H_2O \rightarrow H^+ + OH^- \quad (12)$$

**3.7. Anodization of the Alloy.**

Electrochemical oxidation of $CoFe_2$ alloy films prepared at the optimum electrodepositing synthesis parameters was carried out at room temperature (25ºC ). The conversion of $MFe_2$ alloy to the ferrite analogous ($MFe_2O_4$) via the hydroxide form can be traced with the subsequent reaction:

$$MFe_2 + 8OH^- \rightarrow MFe_2O_4 + 4H_2O + 8e^- \quad (13)$$

After oxidation, the hydroxide film was washed by deionized water and then dried in a desiccator. Then, annealing of the hydroxide films should eliminate few defects raised during the electrodeposition and anodization processes, such as holes, grain boundaries, dislocations, stress, etc. Thus, annealing is considered a stress relief and causes local structural rearrangements affecting the stoichiometry of the synthesized film [48]. Therefore, $CoFe_2$ hydroxide precursors were annealed at 400 C for 2hrs in which sharper and more intense diffraction peak were identified due to the (311) plan as expected for spinel structure. Theses observation favors the nucleation and crystallization of a spinel phase after anodization and annealing, respectively [49].

**3.8. Crystal structure.**

Fig. 9 represents the XRD pattern of $CoFe_2O_4$ thin films synthesized using galvanostatic technique. The results indicated that Cubic spinel cobalt ferrite $CoFe_2O_4$ phase was observed. No extra peak related to tetragonal $CoF_2O_4$ was matched. The crystallite size of $CoFe_2O_4$ phase was calculated automatically by the X –ray diffractometer and summarized in Table 3.

| Substrate/crystallite size( nm) | Pt | SS | Cu |
|---|---|---|---|
| Galvanostatically | 43 | 77 | 102 |

The resulted film was prepared using cathodic current density 100 $mAcm^{-2}$ on Pt, SS and Cu substrate and annealed at 400 $^0$C. Typical diffraction peaks for $CoFe_2O_4$ were indexed and corresponding to diffraction planes of (311), (511) and (440) on Pt substrate as shown in Figure 9 Pt. While relatively sharp peaks favors crystalline state of $CoFe_2O_4$, the planes were indexed corresponding to the diffraction planes of (111), (220), (311), (440) and (533) formed on SS substrate as shown in Figure 9 SS. Moreover, at Figure 9 Cu, the strong sharp peaks of the resulted film demonstrate a good crystalline state of the cobalt ferrite film as formed film on copper substrate with a diffraction planes of (220) (311) (531) (533) and (622).

| Pt | SS | Cu |
|---|---|---|
| 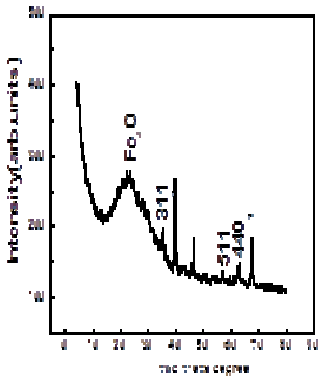 | 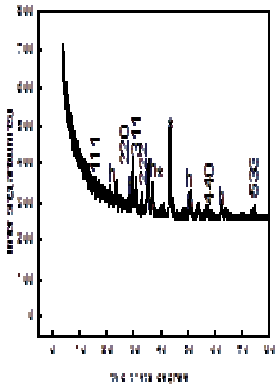 | 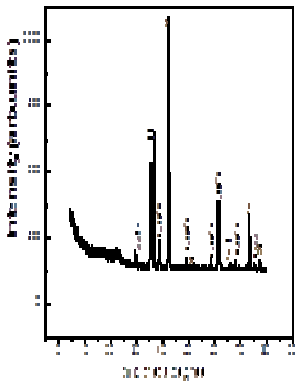 |

**Fig. 9. XRD patterns of $CoFe_2O_4$ electrodeposited from sulfate bath at current density -100 mA $cm^{-2}$ deposited on different substrates at 400 $^0$c.**

### 3.9. Microstructure.

Fig.10 shows the SEM micrographs of cobalt ferrite films prepared on different substrates at –100 $mAcm^{-2}$. The prepared films were annealed at 400 0C for 2 hrs. The micrographs of cobalt ferrite films show a dendritic like structure with a good agglomeration with Pt substrate but in st.st substrate films shows spongy semicircular .Moreover, films deposited on Cu substrate shows rocky like structure with stone edges. [46]

| substrate | SEM micrographs of cobalt ferrite films |
|---|---|
| Pt | 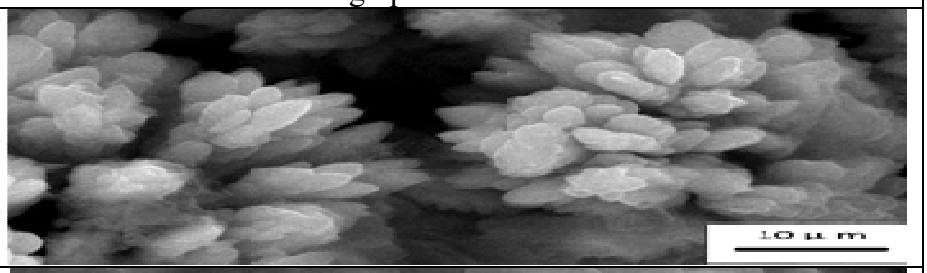 |
| SS | 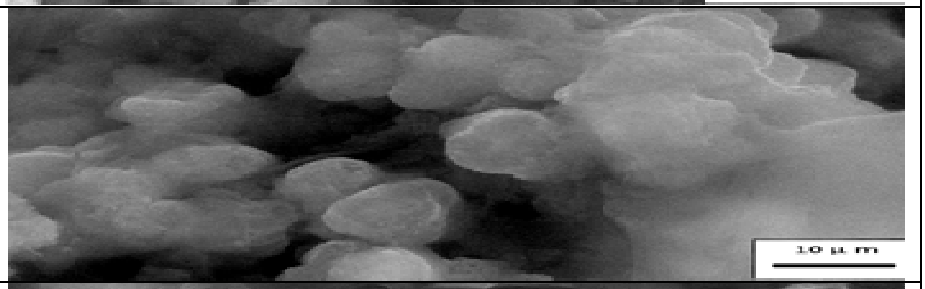 |
| Cu | 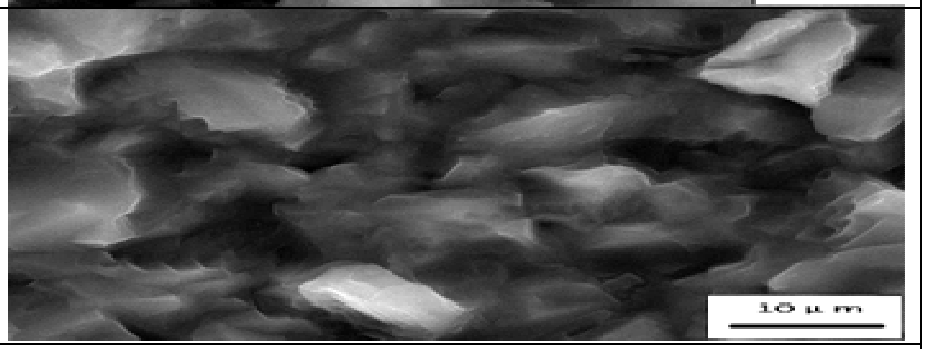 |

**Fig. 10. SEM image of cobalt ferrite thin film electrodeposited from sulfate bath at Current density -100 $mAcm^{-2}$ deposited on different substrates at (400 $^0$c) for 2 hrs.**

### 3.10. Magnetic properties.

The plots of M–H loops for annealed cobalt ferrite thin films are described in Fig.11 (A- C).

The Ms and Mr values were enhanced by increasing the annealing temperature from 400 to 800°C which arising from the spin non-colinearity at crystals surface (Table 4). Moreover, the shifts in the magnetic properties of the samples could be attributed to the reformation of the crystallinity and crystallite sizes changes. The energy of a magnetic particle in an external field is proportional to its particle sizes. Therefore, the decrease of the Ms Values upon decreasing particle sizes can be attributed to surface effects as a result of finite-size scaling of nano crystallites [50-52].

Moreover, saturation magnetization is directly proportional to temperature, as calcination temperature increases the inter- and intra- granular holes decreases. These holes produce a gap that inhibits the movement of domain walls. Remnant magnetic induction shows a very small change with temperature, on the other hand, the coercive force decreases clearly with increasing temperature .

**Table 4: Effect of annealing temperatures on the magnetic properties of different substrates**

| substrate | Pt | | | SS | | | Cu | | |
|---|---|---|---|---|---|---|---|---|---|
| T °C | $M_s$(emu/g) | $M_r$(emu/g) | $H_c$(G) | $M_s$(emu/g) | $M_r$(emu/g) | $H_c$(G) | $M_s$(emu/g) | $M_r$(emu/g) | $H_c$(G) |
| 400°C | 17 | 5.63 | 352 | 20 | 15.2 | 1113 | 9 | 4.07 | 744 |
| 600°C | 29 | 7.02 | 277 | 33.6 | 30.2 | 824 | 31.65 | 15.84 | 433 |
| 700°C | 52 | 7.66 | 55 | 41.96 | 37.22 | 680 | 35 | 21.08 | 215 |
| 800°C | 64.33 | 8.45 | 98 | 54.7 | 49.54 | 522 | 54.5 | 40.2 | 85 |

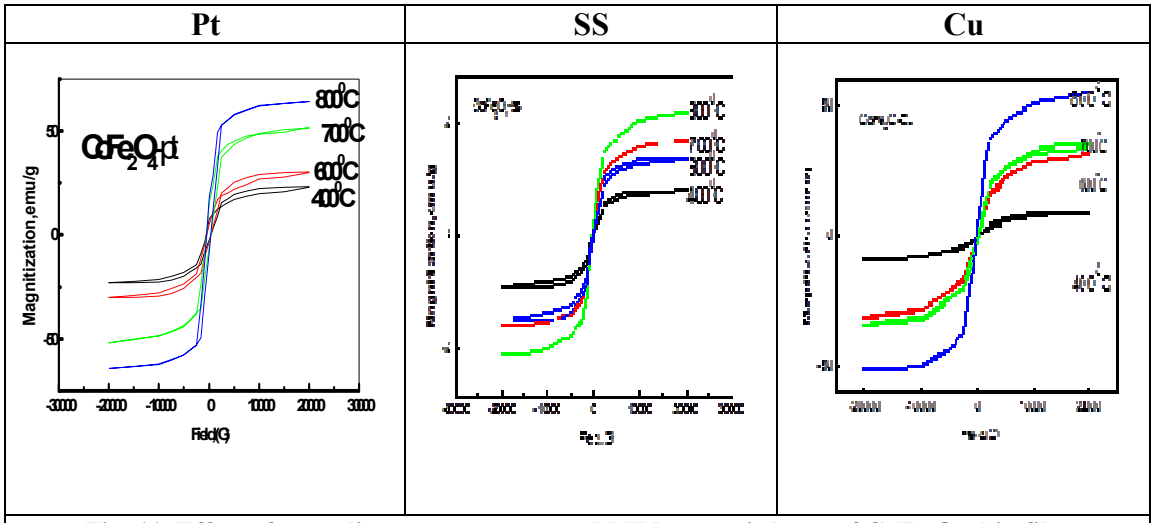


**Fig. 11. Effect of annealing temperatures on M-H hysteresis loops of $CoFe_2O_4$ thin film electrodeposited from sulfate bath at current density -100 mAcm$^{-2}$ on different substrates at annealing temperatures (400 $^0$c, 600 $^0$c, 700 $^0$c , and 800$^0$c)**

### Conclusions

The results can be summarized as follows:

- Cobalt ferrite has been successfully synthesized employing electrodeposition–anodization process.
- Electrodeposited $CoFe_2O_4$ was produced from aqueous sulphate bath at a cathodic Current density 100 mAcm$^{-2}$ at different substrates (Pt, SS, Cu) with a high around current efficiency( 98% , 93%, 86%) respectively.
- The results revealed that agitation has improved effect on current density but had opposite effect on film adhesion
- The results also exposed that bath temperature had strong pushing effect on cobalt ferrite deposition.
- Increasing the deposition current causes an increase in the thickness of the deposited film and optimum current efficiency satisfied at cathodic current density 100 mA cm$^2$.
- According to XRD patterns the prepared film was cobalt ferrite with spinel crystal structure, the crystallite size was 43 nm for cobalt ferrite on Pt substrate, 77 nm on stainless steel and 102 nm on copper substrates annealed at 400 $^0$ C for 2 hrs. predicted the film was nanocrystalline.
- According to theoretical SH model it is observed that the nucleation and growth mechanism prevailed experimentally instantaneous nature at lower and higher potentiostatic condition from -1.5V to -3V at Pt substrate.

- SEM micrographs showed that compact crystallite shapes with smallest particle size and full covered surface and shows agglomeration structure morphology with a narrow distribution of the particles noted, with an average particle size of 4μm for cobalt ferrite on Pt substrate ,12 μm on SS and 9 μm on Cu substrates annealed at 400 $^0$ C for 2 hrs.
- The magnetic properties of the nano composite samples are strongly affected by the calcination temperature as a consequence of crystallinity increase and particle size growth. These materials have good potential in technological applications

## REFERENCES


1) MS Cortés, A Martinez-Luevanos, LA Garcia-Cerda, 2015. Nanostructured pure and substituted cobalt ferrites: fabrication by electrospinning and study of their magnetic properties. Journal of Alloys and Compounds, 653: 290-297.
2) A Amirabadizadeh, Z Salighe, R Sarhaddi, Z Lotfollahi, 2017. Synthesis of ferrofluids based on cobalt ferrite nanoparticles: Influence of reaction time on structural, morphological and magnetic properties. Journal of Magnetism and Magnetic Materials, 434: 78–85.
3) A.Vinosha , A Mely , E Jeronsia , K Raja, QS Tamilarsi ,Ac Fernandez, S Krishnan , S J Das, 2016 . Investigation of optical, electrical and magnetic properties of cobalt ferrite nanoparticles by naive coprecipitation technique, International Journal for Light and Electron Optics, 127, 9917–9925.
4) M Ristic, S Krehula, M Reissner, M Jean, B Hannoyer, S Music, 2017. Synthesis and properties of precipitated cobalt ferrite nanoparticles, Journal of Molecular structure, 1140: 32-38.
5) LB Zakiyah, E Saion ,NM AlHada ,E Gshahi ,A Salem ,N Soltani , S Gene, 2015. Up-scalable synthesis of size-controlled copper ferrite Nano crystals by thermal treatment method, Journal of Materials Science in Semiconductor Processing, 40:564–569.
6) N Debn ,T Kawaguchi ,W Kumasaka , H Das, K Shinozaki , N Sakamoto , H Suzuk ,N Wakiya, 2017. As-grown enhancement of spinodal decomposition in spinel cobalt ferrite thin films by Dynamic Aurora pulsed laser deposition, Journal of Magnetism and Magnetic Materials 432:391–395.
7) V Bilovol ,L G Pampillo, F D Saccone, 2014. Study on target–film structural correlation in thin cobalt ferrite films grown by pulsed laser deposition technique, Journal of Thin Solid Films, 562: 218–222.
8) G Dascalu, G Pompilianb, B Chazallon, OF Caltun, S Gurlui, 2013. Femtosecond pulsed laser deposition of cobalt ferrite thin films, Journal of Applied Surface Science, 278: 38–42.
9) RS Hassan, N Viart, CU Bouillet, J L Loison, G Versini, J P Vola, O Crégut, G Pourroy. , D Muller, D Chateigner, 2007. Structural properties of cobalt ferrite thin films deposited by pulsed laser deposition: Effect of the reactive atmosphere, Journal of Thin Solid Films, 515:2943–2948.
10) AO Cetinkaya, S Kaya, A Aktag, E Budak, E Yilmaz, 2015. Structural and electrical characterizations of BiFeO3capacitors deposited by sol–gel dip coating technique, Journal of Thin Solid Films, 590: 7–12.
11) Le Trong, H Bui, T Presmanes, L Barnabé, A Pasquet, I Bonningue, C Tailhades, 2015. Preparation of iron cobaltite thin films by RF magnetron sputtering. Journal of Thin Solid Films, 589: 292–297.
12) J Xiao, P Liu, C X Wang, G W Yang, 2017. External field-assisted laser ablation in liquid: An efficient strategy for nanocrystal synthesis and nanostructure assembly, Journal of Progress in Materials Science 87:140–220.
13) F C. Ducros, T Schmitt, P Steyer, A Billard, 2011. Nanostructured hard coatings deposited by cathodic arc deposition: From concepts to applications, Journal of Surface & Coating Technology, 205: 5444–5453.
14) M Gharibshahian, O Mirzaeeb, M S Nourbakhsha, 2017. Evaluation of superparamagnetic and biocompatible properties of meso porous silica coated cobalt ferrite nanoparticles synthesized via microwave modified Pechini method, Journal of Magnetism Magnetic Materials, 425: 48–56.
15) F Tudorache,P D Popa, M Dobromir, F Iacomi, 2013. Studies on the structure and gas sensing properties of nickel–cobalt ferrite thin films prepared by spin coating, Journal of Materials Science and Engineering: B, 178: 1334–1338.
16) J Sun, Z Wanga, Y Wang, Y Zhu, T Shen, L Pang, K Wei, F Li, 2012 . Synthesis of the nanocrystalline $CoFe_2O_4$ ferrite thin films by a novel sol–gel method using glucose as an additional agent, Journal of Materials Science and Engineering: B, 177: 269–273.

17) CD Lokhande, S S Kulkarni, RS Mane, SH Han, 2007. Copper ferrite thin films: Single-step non-aqueous growth and properties, Journal of Crystal Growth, 303:(2): 387–390.

18) E M Elsayed , M M Rashad , H F Y Khalil ,I A Ibrahim, M R Hussein ,M M B El-Sabbah , 2016 . The effect of solution pH on the electrochemical performance of nanocrystalline metal ferrites $MFe_2O_4$ (M=Cu, Zn, and Ni) thin films, Journal of Applied Nanoscience, 6: 485–494.

19) SD Sartale, C D Lokhand, M Muller, 2003. Electrochemical synthesis of nanocrystalline $CuFe_2O_4$ thin films from non-aqueous (ethylene glycol) medium, Journal of Materials Chemistry and Physics, 80:120-128.

20) Z Abdel-Hamid, M M Rashad, SM Mahmoud, AT Kandil, 2017. Electrochemical hydroxyapatite-cobalt ferrite nanocomposite coatings as well hyperthermia treatment of cancer, Journal of Materials Science and Engineering: C, 76: 827–838.

21) AR Sadrolhosseini, M Naseri, H M Kamari, 2017. Surface plasmon resonance sensor for detecting of arsenic in aqueous solution using polypyrrole-chitosan-cobalt ferrite nanoparticles composite layer, Journal of Optics Communications 383: 132–137.

22) C D Lokhande, S S. Kulkarni, RS Mane, K C Nandi, S-H Han, 2008. Structural and magnetic properties of single-step electrochemically deposited nanocrystalline cobalt ferrite thin films, Journal of Current Applied Physics, 8: 612–615.

23) F Nana, T Nobuki, S Satoshi, 2010. Preparation of Composite Nanoparticles Based on Cobalt Ferrite Journal of the Japan Institute of Metals, 74: 345-350.

24) IH Gul, A Maqsood, M Naeem, AM Naeem, 2010. Optical, magnetic and electrical investigation of cobalt ferrite nanoparticles synthesized by co-precipitation route, Journal of Alloys and Compounds, 507: 201-206.

25) R Arulmurugan, G Vaidyanathan, S Sendhilnathan, B Jeyadevan, 2005. Preparation and properties of temperature-sensitive magnetic fluid having $Co_{0.5}Zn_{0.5}Fe_2O_4$ and $Mn_{0.5}Zn_{0.5}Fe_2O_4$ nanoparticles, Physica B: Condensed Matter,368:223-230

26) F Tudorache, E Rezlescu, PD Popa, N Rezlescu, 2008. Study of some simple ferrites as reducing gas sensors Journal of OptoElectronics and Advanced Materials, 10: 1889-1893.

27) MM Rashad, RM Mohamed, M A Ibrahim, L F M Ismail, E A Abdel-Aal, 2012. Magnetic and catalytic properties of cubic copper ferrite nanopowders synthesized from secondary resources, Advanced Powder Technology, 23: 315–323.

28) L Jaswala, B Singh, 2014. Ferrite materials: A chronological review Achronological review. Journal of integrated science and technology, 2:(2): 69-71.

29) S Singh, BC Yadav, R Prakash , B Bajaj ,JR lee , 2011 . Synthesis of nanorods and mixed shaped copper ferrite and their applications as liquefied petroleum gas sensor, Journal of Applied Surface Science , 257: 10763–10770.

30) S Bakhshayesh, H Dehghani, 2014. Nickel and cobalt ferrites nanoparticles: synthesis, study of magnetic properties and their use as magnetic adsorbent for removing lead(II) ion, Journal of the Iranian Chemical Society:11, 769–780.

31) M Gharagozloua, B Ramezanzadeh, Z Baradaran, 2016. Synthesize and characterization of novel anticorrosive cobalt ferrite nanoparticles dispersed in silica matrix ($CoFe_2O_4$-$SiO_2$) to improve the corrosion protection performance of epoxy coating, Journal of Applied Surface Science, 377: 86–98.

32) AR Sadrolhosseini, M Naseri, HM Kamari, 2017. Surface plasmon resonance sensor for detecting of arsenic in aqueous solution using polypyrrole-chitosan-cobalt ferrite nanoparticles composite layer, Journal of Optics Communications, 383: 132–137.

33) O Olawale. Ajibol, T Daniel. Oloruntoba, 2014. Effects of polishing grades and Saccharin-550 additive on copper electroplating on NST60Mn and $NST50^{-2}$ steelsInternational Journal of Innovation and Scientific Research 8, ( 2 ): 334-344.

34) P patnaik, St Kumar padhy, B C tripathy, IN nhattacharya, RK paramguru, 2015. Electrodeposition of cobalt from aqueous sulphate solutions in the presence of tetra ethyl ammonium bromide, Transactions of Nonferrous Metals Society of China, 2047-2053.

35) M Nagasaka, H Yuzawa, T Horigome, A P Hitchcock, N Kosugi, 2013. Electrochemical Reaction of Aqueous Iron Sulfate Solutions Studied by Fe L-Edge Soft X-ray Absorption Spectroscopy, Journal of Physical Chemistry: C, 117: 16343−16348.

36) Y Na, Nu Li, Qi-Z Qina, 2005. Nanocrystalline transition metal ferrite thin films prepared by an electrochemical route for Li-ion batteries, Journal of Power Sources, 142, 292–297.

37) T Yoshida, D Komatsu, N Shimokawa, 2004. Mechanism of cathodic electrodeposition of zinc oxide thin films from aqueous zinc nitrate baths, Thin Solid Films, 166:451-452.

38) E M.Elsayed, A E Shalan, M M Rashad, 2014. Preparation of ZnO nanoparticles using electrodeposition and co-precipitation techniques for dye-sensitized solar cells applications, Journal of Materials Science: Materials in Electronics, 25: 3412-3419.

39) SD Sartale, C D Lokhande, 2000. Room temperature preparation of $NiFe_2O_4$ thin films by electrochemical route Indian Journal of Engineering and Materials Science, 7, 404-410.

40) J Stephen. Percival, Zhang, 2014. Study of the Formation and Quick Growth of Thick Oxide Films Using Platinum Nanoelectrodes as a Model Electrocatalyst, Langmuir 30, 11235−11242.

41) D Grieshaber, R MacKenzie, J Vörös, E Reimhult, 2008. Electrochemical Biosensors - Sensor Principles and Architectures, E. Journal of Sensors 8, (3): 1400-1458.

42) Y Kim, J Jung, S Kim, W S Chae, 2013. Cyclic Voltammetric and Chronoamperometric Deposition of CdS Materials Transactions 54, (8): 1467 - 1472.

43) MM Moharam, EM Elsayed, JC Nino, RM Abou-Shahba, MM Rashad, 2016. Potentiostatic deposition of $Cu_2O$ films as p-type transparent conductors at room temperature, Journal of Thin solid Films, 616: 760–766.

44) EM. Elsayed, A E Saba, 2009. P reparation of standard copper ferrite thin film from aqueous solution, Steel Grips,7, 137-141.

45) A saba, E Elsayed, M Moharm and M M Rashad, 2012. Electrochemical Synthesis of Nanocrystalline $Ni_{0.5}Zn_{0.5}Fe_2O_4$ Thin Film from Aqueous Sulfate Bath, ISRN Nanotechnology, 2012: Article ID 532168, 8 pages.

46) A E Saba, E M Elsayed, M M Moharam, M M Rashad, R M Abou- Shahba, 2011. Structure and magnetic properties of $Ni_xZn_{1-x}Fe_2O_4$thin films prepared through electrodeposition method, Journal of Materials Science, 46:3574-3582.

47) AI Inamdar, SH Mujawar, SB Sadale, AC Sonavane, M B Shelar, PS Shinde, PS Patlil, 2007. Electrodeposited zinc oxide thin films: Nucleation and growth mechanism. Journal of Materials Chemistry 91: 864–870.

48) C Dong, G Wang, D Guo, C Jiang, D Xue, 2013. Growth, structure, morphology, and magnetic properties of Ni ferrite films, Nanoscale Research Letters, 8:196.

49) Maria, S Gheorghe, M Magdalena, Traian, 2010. Roznov pod Radhostem, Synthesis And Characterization Of Nickel Iron Alloys By Electrodeposition Czech Republic, EU, 5: 18 - 20.

50) SD Sartale, CD Lokhande 2002. Electrochemical synthesis of nanocrystalline $CoFe_2O_4$ thin films and their characterization. Ceramics International 28 (5): 467-477.

51) JL Gunjakar, AM More, VR Shinde, CD Lokhande, 2008 Synthesis of nanocrystalline nickel ferrite ($NiFe_2O_4$) thin films using low temperature modified chemical method, Journal of Alloys and Compounds,465,(1):468-473.

52) M Gharagozlou 2011. Influence of calcination temperature on structural and magnetic properties of nanocomposites formed by Co-ferrite dispersed in sol-gel silica matrix using tetrakis (2-hydroxyethyl) orthosilicate as precursor Chemistry Central Journal, 19:5.